# Three-dimensional reconstruction of the Ribosome from *Escherichia coli*

Terence Wagenknecht, Jose María Carazo, Michael Radermacher, and Joachim Frank
Wadsworth Center for Laboratories and Research, New York State Department of Health, Albany, New York 12201-0509

ABSTRACT Three-dimensional image reconstruction has been applied to electron micrographs of noncrystalline, negatively stained ribosomes obtained from *Escherichia coli*. Several independent reconstructions all show an overall appearance resembling models that had been derived earlier by direct visual interpretation of electron micrographs. The reconstructed ribosomes show numerous structural details not recognized previously, some of which may be functionally significant. A large elongate cavity (~8-nm long × 5-nm wide × 6-nm [maximal] deep) is present on the surface of the ribosome near the base of its stalk and is identifiable as a portion of a feature termed the interface canyon, which was detected in prior reconstructions of the large ribosomal subunit (Radermacher, M., T. Wagenknecht, A. Verschoor, and J. Frank. 1987. *EMBO (Eur. Mol. Biol. Organ.) J.* 6:1107–1114). On the back of the ribosome, near the base of the central protuberance, is a hole leading to the interface canyon, which likely represents an exit site for the elongating polypeptide produced during protein biosynthesis. The exposed portion of the interface canyon appears well suited to bind two tRNA molecules in a configuration that is consistent with biochemical and structural data on the mechanism of peptide bond biosynthesis.

## INTRODUCTION

Current models for the three-dimensional (3D) architecture of the prokaryotic ribosome are based mainly upon visual interpretation of electron micrographs of the ribosome and its component subunits. Unfortunately, the existing structural models of the ribosome differ significantly from one another, and this often precludes an unambiguous correlation of electron microscopic results with those from other structural and functional studies (for a review, see Wittman, 1983). For example, at least three different arrangements have been proposed for the locations and orientations of the acceptor- and peptidyl-tRNA molecules on the surface of the ribosome (Lake, 1977; Spirin, 1983; Ofengand et al., 1986), and this is due, in part, to the fact that different structural models of the ribosome were used.

To extract fully the information contained in electron micrographs, and to avoid subjective interpretations, which are largely responsible for the discrepancies among the existing structural models of the ribosome, quantitative 3D reconstruction is required. Recently we described a new method of reconstruction that does not require crystalline specimens, as in most conventional methods, but instead uses images of individual macromolecular complexes (Radermacher et al., 1987*a*, *b*; Frank et al., 1988). Here we have used this method to determine the first quantitative 3D reconstruction of the ribosome from *Escherichia coli*. The most intriguing structural feature of the reconstruction is a cavity near the putative location of the peptidyl transferase center that is large enough to accommodate the aminoacyl stems of two, and possibly three, tRNA molecules. A preliminary account of this work has appeared (Wagenknecht et al., 1987).

## MATERIALS AND METHODS

Tight-couple ribosomes were prepared from frozen cells of *E. coli* MRE600 (Robertson and Wintermeyer, 1981) which were obtained from Grain Processing (Muscatine, IA). The ribosomes were stored frozen in aliquots from which further purification was achieved immediately before electron microscopy by sucrose density-gradient centrifugation (10–30% wt/vol sucrose in 20 mM Tris [pH 7.5], 10 mM $MgCl_2$, 100 mM $NH_4Cl$, 0.5 mM EDTA, 3 mM 2-mercaptoethanol). The ribosomes were applied to 300-mesh grids covered with a thick fenestrated layer of carbon, and negatively stained (uranyl acetate, 0.5%, pH not adjusted) by a "sandwich" technique (Stöffler and Stöffler-Meilicke, 1983).

Electron microscopy was performed using a Philips EM420T transmission electron microscope equipped with a low dose kit and eucentric goniometer. Each specimen field was photographed twice at an instrumental magnification of 49,000: first, with the specimen grid tilted by 50° and second, with the grid untilted (Fig. 1, *a* and *b*). Specimens prepared in the manner described above often exhibit severe drift when recorded with minimal electron dose (~1,000 e/nm$^2$). Consequently, we found it necessary to preirradiate the specimen briefly (2–3 s) before recording the micrographs (1-s exposure). Thus the micrographs of the tilted specimen endured a net dose of 30–40 e/nm$^2$, whereas those of the untilted specimen (which are not used in computing the 3D reconstruction) were exposed to an additional 50 e/nm$^2$. Radiation damage to the specimen is unlikely to be the resolution-limiting factor in this study (see discussion of 3D resolution below). A total of 63 tilt/untilt pairs of micrographs were collected. These were screened by optical diffraction

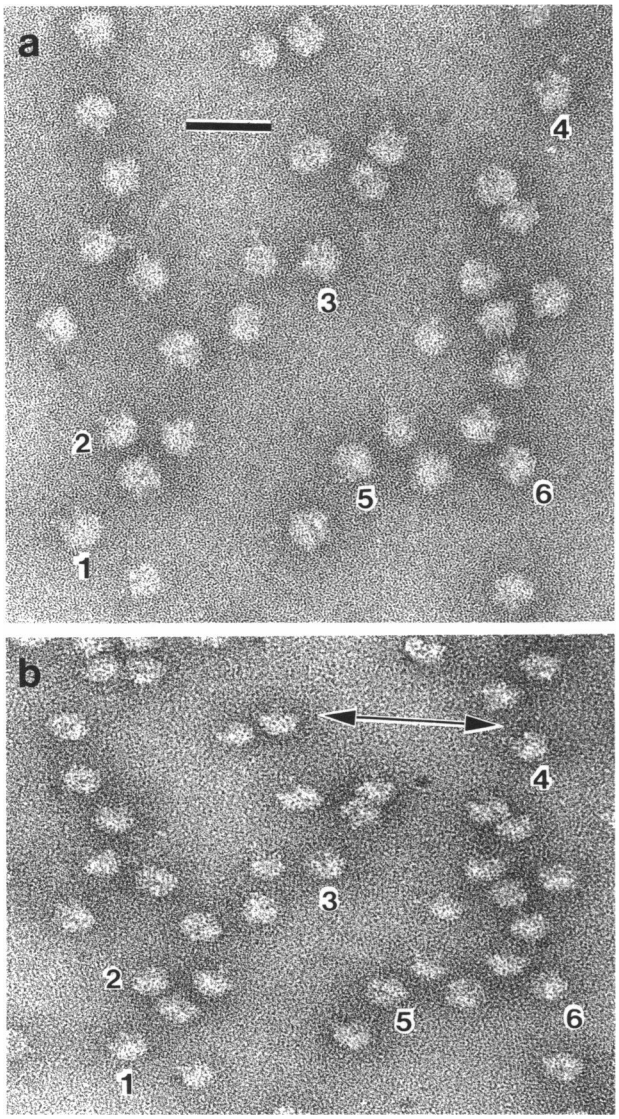


FIGURE 1 Electron micrographs of negatively stained ribosomes. (*a*) Specimen untilted; (*b*) same field as *a* but with grid tilted by 50°. Some of the overlap images in *a* and *b* are numbered. Scale bar represents 50 nm. Arrow in *b* denotes direction of tilt axis.

for appropriate defocus and acceptable levels of drift and astigmatism, and also visually for uniform stain spreading and thickness. Five such pairs of micrographs were finally selected for the analysis described.

The method of 3D reconstruction used has been described previously (Radermacher et al., 1987*b*; Frank et al., 1988). Briefly, the method makes use of the fact that, when tilted in the electron microscope, particles which absorb to the grid in a preferred orientation effectively constitute a conical tilt series of the specimen from which a 3D reconstruction can be computed; we have used a generalized weighted back-projection algorithm described by Radermacher et al. (1987*b*).

Negatively stained ribosomes often assume a characteristic orientation on the electron microscope grid, giving rise to the so-called overlap view (Lake, 1976, see numbered images in Fig. 1 *a*), which is suitable for our method of 3D reconstruction. However, this view is not homogeneous and it appears to comprise a range of orientations related primarily by rotations about a single axis (Verschoor et al., 1986; Carazo et al., 1989). To obtain a more homogeneous set of images, multivariate statistical (correspondence) analysis (MSA; van Heel and Frank, 1981; Frank and van Heel, 1982) was carried out on the aligned set of images obtained from the untilted micrographs. We found, in agreement with a previous study (Verschoor et al., 1986) that the first (largest) eigenvector, which accounted for 13% of the interimage variation, was explicable in terms of a "rocking" of the ribosomes about the axis mentioned above.

From the MSA various subsets of images were identified, and 3D reconstructions were determined for each (see companion paper by Carazo et al., 1989), for details of the classifications). Here, we focus primarily on one of the reconstructions, hereafter referred to as the central reconstruction, so-called because it is derived from those images that lie near the origin (within one standard deviation) of the axis defined by the first eigenvector. The number of images of tilted ribosomes incorporated into the reconstruction was 242. Fig. 2, *a* and *b* shows two averages obtained for independent subsets ($n = 121$) of the images from the untilted specimen micrographs that correspond to those images from the tilted micrographs actually used for determining the 3D reconstruction. These averages were determined to gain some understanding of the actual preservation of structural detail throughout the selected set of images, which, according to a phase-residual analysis (Frank et al., 1981) is 3.0 nm. Probably the principal resolution-limiting factor is the residual inhomogeneity of the images since reproducibilities of 2 nm or better have been routinely obtained for averaged images of the large ribosomal subunit (Radermacher et al., 1987*a*). Generally, the resolution of a 3D reconstruction will be somewhat lower than that obtained for the 2D averages (see Radermacher et al., 1987*b*) and, indeed, the resolution obtained for the central 3D reconstruction was determined to be 4.5 nm by phase-residual analysis and 3.5 nm by the Fourier ring-correlation test (Saxton and Baumeister, 1982; van Heel et al., 1983) of corresponding slices of two independent reconstructions (Radermacher et al., 1987*b*).

Since only the images of the tilted specimen are used in determining the 3D reconstruction, a further test of the reconstruction is to compare its projection in the view corresponding to that of the untilted ribosomes (i.e., the "overlap" view) with the projection obtained by directly averaging the images of the untitled particles. This comparison is made in Fig. 2 where it is seen that the projection computed from the 3D map (Fig. 2 *d*) agrees well with that obtained by averaging the untilted ribosomal images (Fig. 2 *c*).

In addition to the central 3D reconstruction, we will also refer to one other reconstruction that was determined for images lying near one extreme of the first eigenvector direction. In the companion paper by Carazo et al. (1988*b*) this reconstruction is referred to as the "far-o" reconstruction. The differences among the 3D reconstructions can give valuable information on the nature of any orientation-dependent distortions endured by the particles during adsorption and drying. Also certain structural features are resolved more clearly in some reconstructions than in others. Although an accurate estimate of the reproducibility of the "far-o" reconstruction could not be assessed by the methods used for the central reconstruction due to the limited number of images, $n = 89$, it was estimated that the resolution was in the range of 4–5 nm. Accordingly, both 3D reconstructions of the ribosome have been low-pass filtered to a limiting resolution of 4.5 nm in the representations shown in Figs. 3–5.

## RESULTS

Surface representations of the ribosome from the central reconstruction (see Materials and Methods section) are

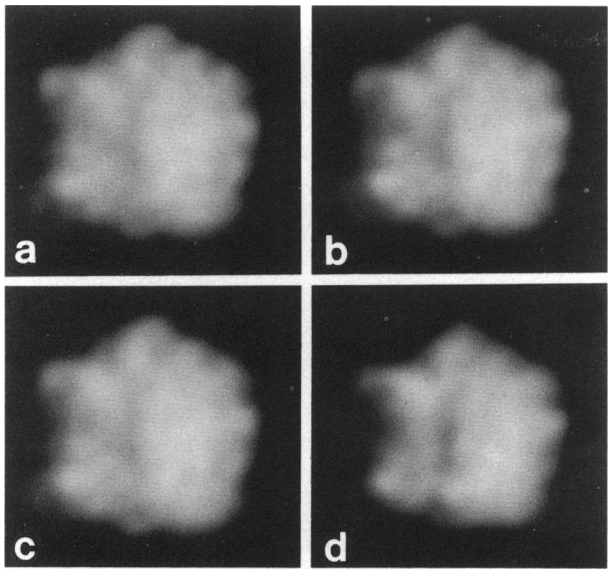


FIGURE 2 Projection images of the ribosome in the overlap orientation. (*a* and *b*) Two independent averaged images of untilted ribosomes obtained after selection and alignment of particles from the five micrographs used in the analysis ($n = 121$ for each). (*c*) The total average for all 242 particles. (*d*) The central 3D reconstruction projected in the overlap orientation. Note the close agreement with the averaged 2D image in *a*–c. *a*–c were low-pass filtered to a limiting resolution of 3 nm whereas *d* was filtered to 4.5 nm, the estimated resolution of the 3D reconstruction. Width of each frame is 33 nm.

shown in Fig. 3 *a*. By comparing the previously reconstructed large ribosomal subunit (Fig. 3 *c*, Radermacher et al., 1987*a*) with the complete ribosome (Fig. 3 *b*) in equivalent orientations, the relative positions and orientations of the large (50S) and small (30S) subunits in the ribosome become apparent. The 30S subunit in Fig. 3 *b* (see also Fig. 4 *a*) lies on top of the 50S subunit along its left side leaving a large portion of the right-hand side of the 50S subunit not covered by the 30S subunit. The overall appearance of the reconstructed ribosome and its constituent subunits agrees generally with the majority of the models derived by visual inspection of electron micrographs (reviewed by Wittman, 1983).

## Structure of the small subunit

When the ribosome is viewed in the overlap orientation (Figs. 3 *b* and 4 *a*), the 30S subunit clearly appears in a characteristic orientation, termed the asymmetric view by Lake (1976) and the angled asymmetric view by Stöffler and Stöffler-Meilicke (1986), that had been identified in electron micrographs of isolated 30S subunits. The head of the 30S subunit extends from the central protuberance to the L1 ridge feature of the 50S subunit, while the main body of the small subunit (*H* and *B*, respectively, in Figs. 3 *b* and 4 *a*) extends to slightly beyond the bottom of the large subunit.

We do not observe a prominent cleft near the middle of the 30S particle resembling those present on some visually derived models, but if such a feature exists and faces the 50S subunit, it might not have been resolved in the reconstruction (see discussion of interface region below). Notably the morphology of this region of the small subunit is the most variable among the various visually derived models (Wittman, 1983). In the 3D reconstruction a small cleft is, however, present on the right side of the small subunit at the juncture of the head and base; possibly it actually extends further into the interface between the two subunits than is resolved in the reconstruction. Also, two lobes of stain-excluding material are present on the left side of the 30S subunit (*BP* in Figs. 3 *b* and 4 *a*) that appear analogous to a single lobe referred to variously in the visually derived models as the "large lobe" (Stöffler and Stöffler-Meilicke, 1986), "platform" (Lake, 1976; Oakes et al., 1986), or "side bulge" (Vasiliev, 1974).

The thickness of the 30S subunit (i.e., its dimension in the direction normal to the overlap [0° and 180°] views of the ribosome) appears variable along its length and somewhat lower than expected (see third views from left in rows 1 and 2 of Fig. 3 *a*). The overall thickness of the reconstructed ribosome in regions where the small subunit is present is only 2–4 nm greater than that of the independently reconstructed 50S subunit (Radermacher et al., 1987*a*). Furthermore, at the junction of the head and body of the 30S subunit, the thickness is not significantly greater than that of the 50S subunit alone. A similar constriction at the head/body junction of the small subunit is also present in the recently reported 3D reconstruction of the ribosome from *Bacillus stearothermophilus* (Arad et al., 1987).

## Structure of the large subunit

The most distinctive feature of the large subunit as it appears in the reconstructed ribosome is a large cavity, ~8-nm long × 5-nm wide × 6-nm (maximal) deep, which is located between the small subunit and the L7/L12 stalk of the large subunit (*IC* in Figs. 3 *b* and 4 *a*). This cavity is obviously a part of the feature we named the "interface canyon" in the previously determined 3D reconstruction of the isolated 50S subunit (Fig. 3 *c*; Radermacher et al., 1987*a*). In the ribosome the left side of the interface canyon is covered up by the overlying 30S subunit (cf. Fig. 3, *b* and *c*).

Several features of the 50S subunit appear slightly different in the reconstructed ribosome than in the isolated 50S subunit, but overall its structure is remarkably similar in both environments. Both the central protuber-

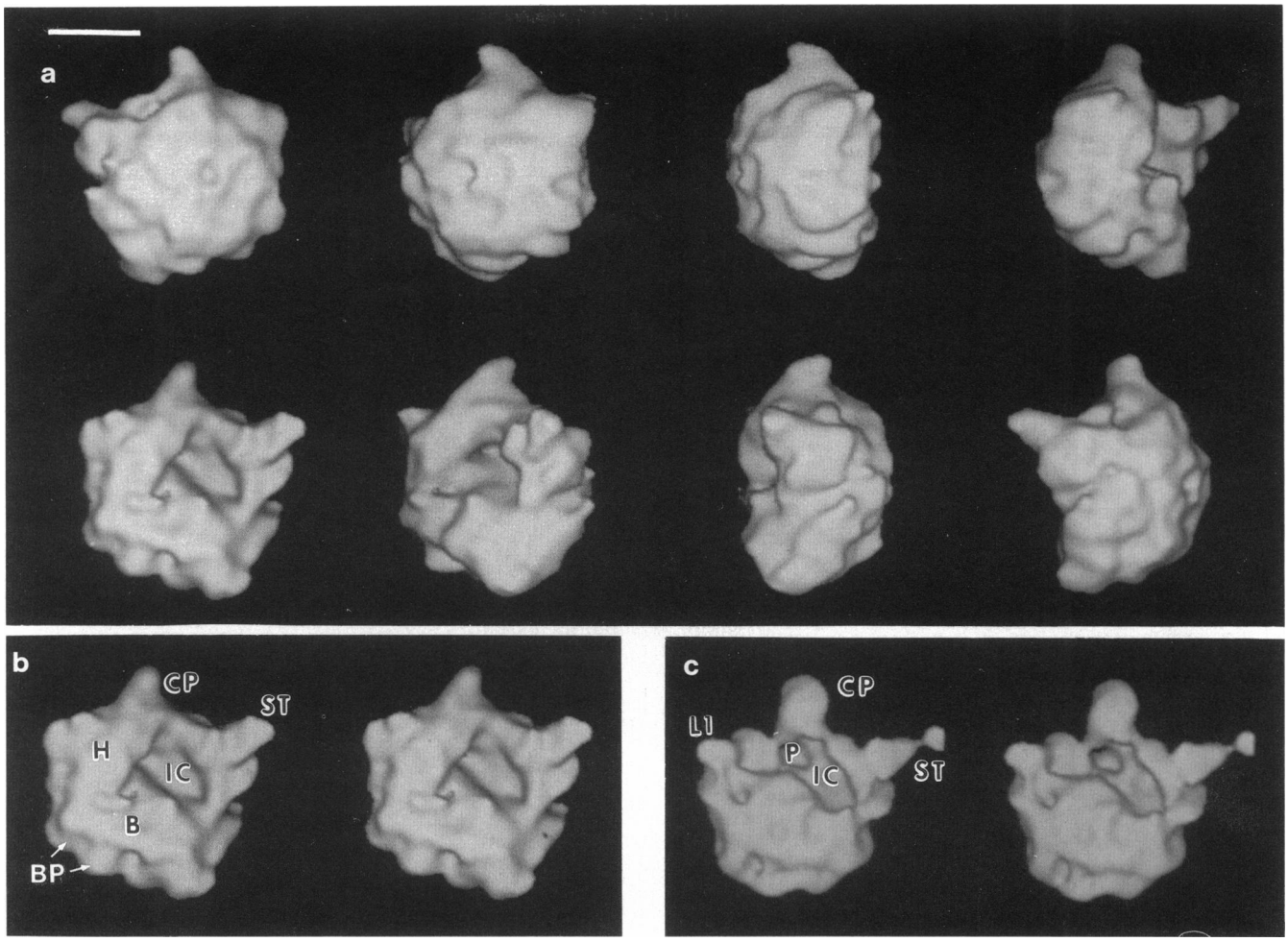


FIGURE 3 Surface representations (Radermacher and Frank, 1984) of the central 3D reconstruction of the ribosome. (*a*) Ribosome in different orientations related by successive 45° rotations about a vertical axis. (*b*) Stereo pair of ribosome in the overlap orientation. (*c*) Stereo pair of 50S subunit (filtered to 3 nm resolution) reconstructed previously (Radermacher et al., 1987*a*, *b*). The density threshold chosen for the surfaces in *a* and b was such that the enclosed volume, corresponding to 3,700 $nm^3$, represents ~90% of the volume of the ribosome (as estimated from the experimentally determined volume of the 50S ribosomal subunit [Tardieu and Vachette, 1982; Meisenberger et al., 1984] and assuming a directly proportional increase for the additional mass of the small subunit). *ST*, L7/L12 stalk; *IC*, interface canyon; *CP*, central protuberance of 50S subunit; *P*, hole from interface canyon to back of 50S subunit. *H*, *B*, head and body, respectively, of the 30S subunit;, *BP*, bilobed platform of 30S subunit. Bar, 10 nm.

ance and L7/L12 stalk appear to be tilted forward (i.e., toward the viewer in Fig. 3 *b*) in the ribosome relative to their positions in the isolated 50S subunit (Fig. 3 *c*). The tilting of the stalk, although substantial (~30°), is not nearly as extreme as in the model of the ribosome proposed by Lake (1977; Oakes et al., 1986) in which the stalk bends onto the interface side of the large subunit and terminates at the right side of the small subunit. It is not known whether these changes are induced by the association of the two subunits, or result from differing interactions of the two structures with the supporting film and stain. In either case, this behavior, as well as the lack of resolvable detail at the interface between the subunits, complicates the task of determining the 3D architecture of the 30S subunit by simple subtraction of the reconstructed 50S subunit from the reconstructed ribosome (see Fig. 5 of Carazo and Frank, 1988).

In the previously reconstructed 50S subunit, an interesting structural feature occurs at the base of the central protuberance in the interface canyon: a stain-filled channel leading to the back of the subunit (*P* in Fig. 3 *c*; see discussion of exit site below). This hole is not well-resolved in the central reconstruction of the ribosome shown in Fig. 3, *a* and *b*, but it is clearly resolved in the reconstructions of the ribosome that were carried out over subsets of images that had less interimage variability (see

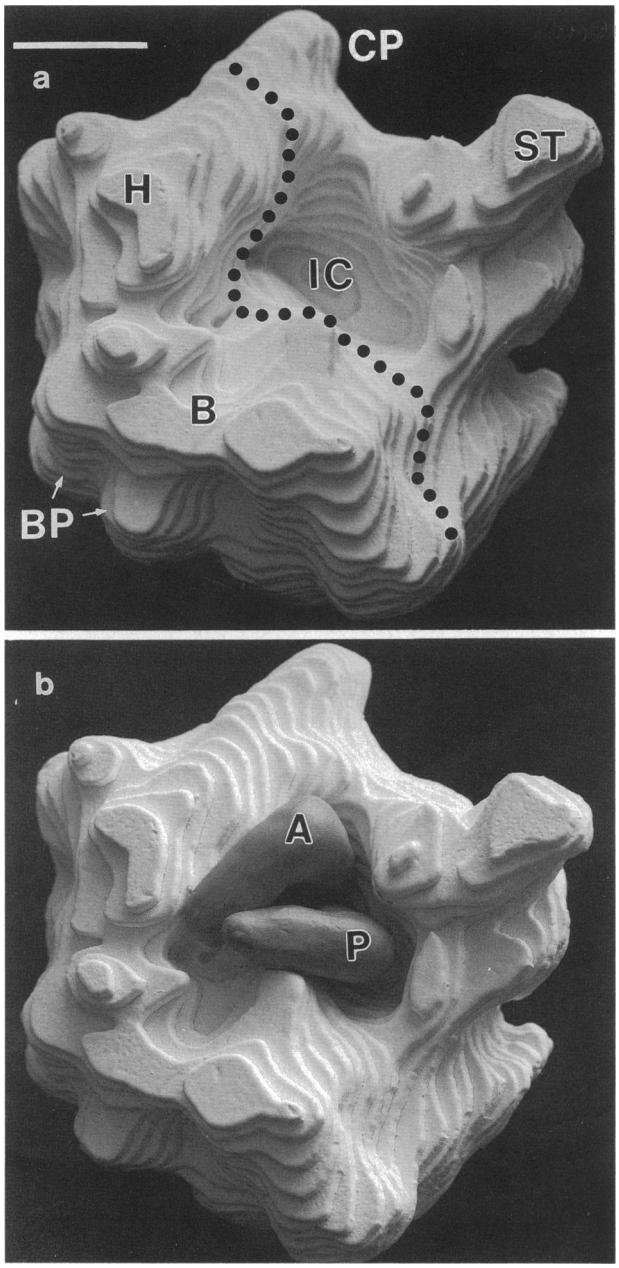


FIGURE 4 Styrofoam models of the 3D reconstruction of the ribosome. (*a*) Ribosome in the overlap orientation. Dashed line indicates boundary between large and small subunits. (*b*) As in *a* but with scale models of two tRNA molecules inserted into the interface canyon. Density threshold and abbreviations as in Fig. 3. Bar, 5 nm.

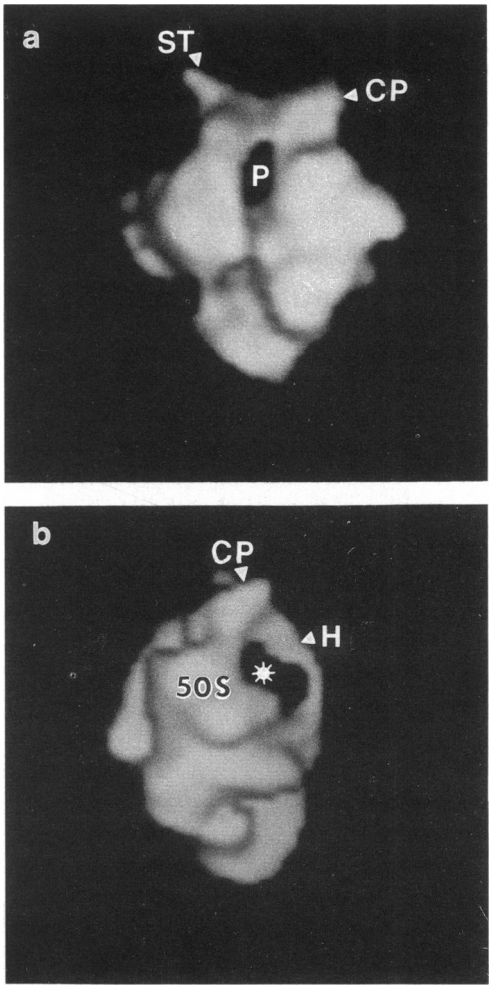


FIGURE 5 Surface representations of the "far left" 3D reconstruction of the ribosome. (*a*) View showing the hole (*P*) on back of 50S subunit. (*b*) View showing stain penetration (*) between the two subunits. Abbreviations as in Fig. 3. The density threshold used is somewhat higher than in the previous figures in order to accentuate these features.

companion paper by Carazo et al., 1989). For example, in the reconstruction obtained for images lying at the extreme left on the first eigenvector axis of the correspondence analysis ("far left" reconstruction), the hole is clearly visible on the back of the ribosome, just below the central protuberance of the large subunit (Fig. 5 *a*).

## The subunit/subunit interface

The central reconstruction shown in Fig. 3, *a* and *b* shows little structural detail in the region between the large and small subunits. There are probably two reasons for this result. First, any collapse or flattening of the ribosome that might have occurred during the drying of the grids will have the effect of pushing the two subunits together, since they lie one on top of the other in the overlap orientation used to determine the reconstruction. Second, the resolution of the 3D reconstructions is always poorest in the direction perpendicular to the grid due to the restricted range of tilting in the electron microscope, and structural details concerning 50S/30S interactions

lie mainly along this direction. One consequence of these considerations, which should be borne in mind when interpreting the intersubunit region of the 3D map, is that there could be more space between the subunits than appears in the 3D reconstruction.

An orientation in which the subunits lie side-by-side on the grid would be more favorable for determining structural details about the 30S/50S interface. Unfortunately, although such orientations occasionally occur, in this study they were not present frequently enough to determine the 3D architecture by the method employed here. However, one of the sub-reconstructions we determined, the "far-o" reconstruction, does show stain extending continuously between the subunits from the interface canyon to the opposite side of the small subunit (Fig 5 *b*). Apparently this is due to a slightly more favorable orientation of the ribosomes comprising this subset of images.

## DISCUSSION

### Comparison with other 3D models of the ribosome

The overall appearance of the three-dimensionally reconstructed ribosome is in basic agreement with the most commonly cited models that have been derived mainly by direct visual analysis of electron micrographs (Stöffler and Stöffler-Meilicke, 1984, 1986; Lake, 1976, 1985; Vasiliev et al., 1983). An important and useful consequence of this concordance with the visually derived models is that the results of the numerous immunoelectron microscopy studies on the prokaryotic ribosome and its subunits can be related directly to the reconstructed ribosome (see discussion of functional implications).

The visually derived models do differ, however, in detail, and the 3D model we have described resolves some of these differences. For example, the reconstructed ribosome shows that substantially more of the interface side of the 50S subunit is not covered by the overlying 30S subunit (Figs. 3 *b* and 4 *a*) than is depicted in the model of Lake (1976). Also, the reconstructions clearly show that the L7/L12 stalk is not folded back onto the interface surface of the large subunit as has been depicted in some representations of the model proposed by Lake (Lake, 1977; 1985; Oakes et al., 1986). This folded configuration of the stalk was proposed originally because the stalk was not clearly visible as a protruding appendage in individual images of the ribosome in the overlap orientation; this is also true of the images that we have analyzed here (Figs. 1 *a* and 2). This feature underscores the necessity of quantitative 3D reconstruction in interpreting electron micrographs of macromolecular complexes. From the 3D reconstruction it can be easily appreciated that the reason that the stalk is not clearly visible in the untitled images is because it is running at an angle to the specimen support (see the 0 and 180° views in Fig. 3 *a*). Thus in the overlap images it appears shorter than its actual length and it is partially overlapped by the main body of the 50S subunit.

The reconstructed ribosome also reveals numerous new structural features, the most striking of which is the interface canyon, which is not present in any of the visually derived models (except perhaps in the model of Stöffler and Stöffler-Meilicke [1984, 1986] which shows a much shorter and shallower groove in this region). As far as we are aware, this is the largest cavity-like feature observed in any biomacromolecular complex (see discussion of functional implications below).

On the 30S subunit portion of the reconstructions there are two lobes of stain-excluding material on its left side (Figs. 3 *b* and 4 *a*), instead of just one as in the visually derived models. Interestingly, several models of the small eukaryotic ribosomal subunit (Boublik et al., 1986; Oakes et al., 1986; Westerman et al., 1986) and one 3D reconstruction (Zhang et al., 1987) show two apparently analogous lobes of material in this region. Thus, a bilobed platform appears to be yet another example of an evolutionarily conserved morphological feature of the small ribosomal subunit (Lake, 1985; Oakes et al., 1986).

Recently, another group (Arad et al., 1987; Yonath and Wittman, 1988) has described a 3D reconstruction of a prokaryotic ribosome at somewhat lower resolution, which shows similarities as well as some distinct differences from the structure we have described and also from the visually derived models. In their reconstructions the 30S subunit has a much thinner, more laterally symmetric appearance than it has in other models, and the L7/L12 stalk appears not to be resolved. Additionally, the interface canyon, which is so conspicuous in our reconstruction, appears not to be clearly resolved in their model (although a groove apparently analogous to the interface canyon does appear in the same group's reconstruction of the 50S subunit [Yonath et al., 1987]). Their model also shows much more solvent-accessible space between the upper half of the 30S subunit and the large subunit than does our reconstruction. Except for the latter difference, which could be due to some flattening or compression of the ribosomes in our preparation (see below), we can only speculate on the reason(s) for these apparent discrepancies. Perhaps one of the methodological differences in the two studies is responsible: ribosomes from different organisms (*E. coli* in our study versus *Bacillus stearothermophilus* in theirs); different organizational states of the specimen (single ribosomes versus

two-dimensional crystals); different methods of electron microscopic data collection (single, low-electron dose exposure per field versus multiple exposures). One should also realize that the appearance of solid-body representations of 3D reconstructions is sensitive to the density threshold chosen for the display, and it might be significant that the volume enclosed by the reconstructions depicted in Arad et al. (1987) is lower than those we have shown; we have also displayed our reconstructions at higher threshold levels (see, for example, Fig. 8 of Carazo et al., 1989) which should be more comparable to those shown in Arad et al. (1987), but little increase in similarity to their model was apparent.

## Flattening and distortion artifacts

A potential complication that arises when attempting to determine the 3D architecture of macromolecular specimens from electron micrographs of isolated, negatively stained macromolecules is that flattening or other distortions can occur when the specimen adsorbs to the specimen grid and is allowed to dry. Distortion effects, as they relate to this study, are discussed in detail in the accompanying paper (Carazo et al., 1989), which concludes that, although some structural deformations do occur, the major structural features resolved in the reconstructions are highly reproducible.

It is difficult to determine the degree of flattening directly from the overall dimensions of the reconstruction because the actual dimensions of the ribosome are not known accurately. We can, however, compare the ratio of the average dimension of our reconstructed ribosome in the direction normal to the grid (i.e., the direction of flattening) to the average dimension parallel to the grid, with the analogous ratio estimated from other models of the ribosome. For our reconstruction the ratio is ~0.65, whereas for the reconstruction of Arad et al. (1987) it appears to be 0.75–0.80, and for the visually derived models it appears to be in the range 0.9–1.0. Thus, our reconstructed ribosome appears to be 10–20% flattened relative to that of Arad et al. and ~30% relative to the visually derived models. It should be appreciated that the ribosomes analyzed by Arad et al. were probably oriented differently with respect to the grid from those in our study, and hence, any flattening that might have occurred in their study would have been in a different direction from that occurring in ours. Therefore, the extent of flattening estimated above for our reconstruction relative to theirs (10–20%), could be an overestimate. Kellenberger et al. (1982) have also shown that ribosomes are relatively resistant to flattening when negatively stained by essentially the same procedure we have used.

## Functional implications

The most intriguing structural feature revealed in our reconstructions is the large cavity present on the portion of the 50S subunit not covered by the 30S subunit as viewed in Fig. 3 *b* and 4 *a*. This cavity is clearly a part of the feature we named the "interface canyon" in the previously determined reconstruction of the 50S subunit shown in Fig. 3*c* (Radermacher et al., 1987*a*; see also Carazo et al., 1988). Two other laboratories, using different methods of 3D reconstruction from that used here, have also described reconstructions of the 50S subunit in which a groove corresponding to the interface canyon is present (Hoppe et al., 1986; Yonath et al., 1987). Recent image-averaging studies carried out in our laboratory on unstained, frozen-hydrated 50S subunits support our interpretation that the interface canyon is a true topographical feature of the subunit and, specifically, that it is not due to positive staining of the rRNA (Wagenknecht et al., 1988*a*).

Several functional sites have been mapped by immunoelectron microscopy to locations in the vicinity of the interface canyon. The elongation factors, EF-G and EF-Tu, both bind to the large subunit near the base of the L7/L12 stalk (Girshovich et al., 1981, 1986) where the interface canyon is most pronounced.

The peptidyl transferase center has been mapped on the 50S subunit just below the central protuberance, somewhere between it and the L1 ridge (Olson et al., 1982; Stöffler and Stöffler-Meilicke, 1984; Lake, 1985). Previously, we observed in the reconstruction of the 50S subunit a hole in the canyon at this location (*P* in Fig. 3 *c*) that leads to the back of the 50S subunit (Radermacher et al., 1987*a*). This hole is not well resolved on the 30S-side of the reconstructed complete ribosome (Figs. 3 *b* and 4 *a*) because of the lower resolution of the latter reconstruction and also due to the presence of the overlying 30S subunit. Yet it is reproducibly resolved on the back side of the reconstructions that were determined using ribosomal images which were more homogeneous in terms of interimage variability than those used for determining the central reconstruction (*P* in Fig. 5; see also companion paper by Carazo et al. [1989]). Previously we hypothesized that this hole on the back of the ribosome represents the site where the growing polypeptide chain escapes initially from the peptidyl transferase center during protein biosynthesis. Direct support for this proposal has been obtained recently in an immunoelectron microscopy study (Ryabova et al., 1988) in which the exiting nascent chain was mapped to a location just below and to the right of the central protuberance when the ribosome is viewed from the back (as in the leftmost image in the top row of Fig. 3 *a*); this is precisely the location of the stain-filled

hole we have detected on the back of the reconstructed 50S subunit and ribosome. Ryabova et al. also detected a secondary exit site for the nascent peptide, located lower down on the back of the large subunit, which agrees well with the results of an earlier immunoelectron microscopy study (Bernabeu and Lake, 1982), and they commented that the two localizations need not be contradictory. For example, the elongating polypeptide might pass through a groove or tunnel that traverses the distance between the two sites and which shields it from reaction with antibodies. In fact, our 3D reconstruction of the large subunit lends support to this hypothesis (Radermacher et al., 1987*a*, 1988).

During protein biosynthesis, tRNA molecules interact with the ribosome at two specific locations known as the acceptor and peptidyl sites (A and P sites), and several hypothetical arrangements have been described for the location and relative orientations of the tRNA's bound at these sites (Lake, 1977; Olson et al., 1982; Spirin, 1983; Ofengand et al., 1986). Given the location of the peptidyl transferase center discussed above and the fact that the anticodons of the tRNA molecules interact with the 30S subunit near the junction of its head and body (for reviews see Ofengand et al., 1986; Oakes et al., 1986; Stöffler and Stöffler-Meilicke, 1986), our 3D reconstruction of the ribosome is consistent with only one general kind of arrangement for the two-ribosome-bound tRNA molecules. A model of this arrangement is shown in Fig. 4 *b*, where the aminoacyl stems of the two tRNA molecules are shown projecting into the interface canyon and directed towards the base of the central protuberance, the putative location of the peptidyl transferase; note that in our 3D reconstruction this is the only possible mode of access to the peptidyl transferase region. The anticodon regions of the tRNA's are shown positioned on the external surface of the 30S subunit near the head–body junction. The angle between the planes formed by the two stems of each tRNA molecule is ~60° in Fig. 4 *b*, but tRNA molecules having larger or smaller angles between them can still fit into the interface canyon. Evidence from fluorescence energy-transfer studies indicates that the angle should be between 30° and 90° (Johnson et al., 1982; Paulsen et al., 1983). Interestingly, this arrangement for the tRNA's is very similar to the arrangement proposed by Spirin (1983). If this model is essentially correct, then the upper tRNA molecule in Fig. 4 *b* is likely in the A-site and the other in the P site (see Spirin, 1983, 1985 for a full discussion of the evidence supporting such an arrangement for the tRNA molecules).

Other proposals for the tRNA positions on the ribosome show the tRNA's accessing the peptidyl transferase center from the left side of the 30S subunit when viewed as in Figs. 3 *b* and 4 (Lake, 1977; Olson et al., 1982; Ofengand et al., 1986). Clearly, our 3D reconstruction, if taken literally, would not allow access by the tRNA molecules from this location to the peptidyl transferase center due to the lack of intersubunit separation (see third and fourth images in first row of Fig. 3). Although the 3D architecture of the ribosome appears to be more compatible with a mode of tRNA binding resembling that hypothesized by Spirin (1983) as discussed above, we do not believe that we can rule out these alternatives models. We have already discussed the likelihood that there might be more solvent-accessible space between the two subunits than is apparent in our 3D reconstruction, and, in fact, one of the reconstructions does show evidence for a channel between the subunits leading to the side of the ribosome where the tRNA's are supposed to bind in the alternative models of tRNA binding (Fig. 5 *b*).

It should now be feasible to map directly the tRNA-binding locations by reconstructing ribosome–tRNA complexes using the methods employed in the present study, and such experiments are now in progress in our laboratory (Wagenknecht et al., 1988*b*). If successful, these studies should, at the very least, allow us to determine on which side of the 30S subunit the tRNA's bind to the ribosome.

The model we have described represents the first objective and quantitative determination of the 3D architecture of the ribosome from *E. coli*. As such, we suggest that it be used in preference to the visually derived models for structure–function correlations.

We thank Adriana Verschoor for discussions.

This work was supported by National Institutes of Health 1R01-029169 and National Science Foundation grant 8313405.

*Received for publication 15 July 1988 and in final form 26 October 1988.*

## REFERENCES

Arad, T., J. Piefke, H. -S. Weinstein, A. Yonath, and H. G. Wittman. 1987. Three-dimensional image reconstruction from ordered arrays of 70S ribosomes. *Biochimie*. 69:1001–1006.

Bernabeu, C., and J. A. Lake. 1982. Nascent polypeptide chains emerge from the exit domain of the large ribosomal subunit: immune mapping of the nascent chain. *Proc. Natl. Acad. Sci. USA*. 79:3111–3115.

Boublik, M., G. T. Oostergetel, J. S. Wall, J. F. Hainfeld, M. Radermacher, T. Wagenknecht, A. Verschoor, and J. Frank. 1986. Structure of ribosomes and their components by advanced techniques of electron microscopy and computer image analysis. *In* Structure, Function and Genetics of Ribosomes. B. Hardesty, and G. Kramer, editors. Springer-Verlag, New York. 68–86.

Carazo, J. M., and J. Frank. 1988. Three-dimensional matching of macromolecular structures obtained from electron microscopy: an application to the 70S and 50S *E. coli* ribosomal particles. *Ultramicroscopy*. 25:13–22.

Carazo, J. M., T. Wagenknecht, M. Radermacher, V. Mandiyan, M. Boublik, and J. Frank. 1988. Three-dimensional structure of 50S Escherichia coli ribosomal subunits depleted of proteins L7/L12. *J. Mol. Biol.* 201:393–404.

Carazo, J. M., T. Wagenknecht, and J. Frank. 1989. Variations of the three-dimensional structure of the *Escherichia coli* 70S monosome in the range of overlap views: an application of the methods of multicone and local single-cone three-dimensional reconstruction. *Biophys. J.* 55:465–477.

Frank, J., and M. van Heel. 1982. Correspondence analysis of aligned images of biological particles. *J. Mol. Biol.* 161:124–137.

Frank, J., A. Verschoor, and M. Boublik. 1981. Computer averaging of electron micrographs of 40S ribosomal subunits. *Science (Wash. DC)*. 214:1353–1355.

Frank, J., A. Verschoor, T. Wagenknecht, M. Radermacher, and J. M. Carazo. 1988. A new non-crystallographic image-processing technique reveals the architecture of ribosomes. *Trends Biochem. Sci.* 13:123–127.

Girshovich, A. S., T. V. Kurtskhalia, Yu A. Ovchinnikov, and V. D. Vasiliev. 1981. Localization of the elongation factor G on Escherichia coli ribosome. *FEBS (Fed. Eur. Biochem. Soc.) Lett.* 130:54–59.

Girshovich, A. S., E. S. Bochkareva, and V. D. Vasiliev. 1986. Localization of elongation factor Tu on the ribosome. *FEBS (Fed. Eur. Biochem. Soc.) Lett.* 197:192–198.

Hoppe, W., H. Oettl, and H. R. Tietz. 1986. Negatively stained 50S ribosomal subunits of Escherichia coli. *J. Mol. Biol.* 192:291–322.

Johnson, A. E., H. J. Adkins, E. A. Matthews, and C. Cantor. 1982. Distance moved by transfer RNA during translocation from the A to the P site on the ribosome. *J. Mol. Biol.* 156:113–140.

Kellenberger, E., M. Haner, and M. Wurtz. 1982. The wrapping phenomenon in air-dried and negatively stained preparations. *Ultramicroscopy*. 9:139–150.

Lake, J. A. 1976. Ribosome structure determined by electron microscopy of Echerichia coli small subunits, large subunits and monomeric ribosomes. *J. Mol. Biol.* 105:131–159.

Lake, J. A. 1977. Ribosome structure and tRNA binding sites. *In* Transfer RNA: Structure, Properties and Recognition. P. R. Schimmel, D. Soll, and J. N. Abelson, editors. Cold Spring Harbor Laboratory, Cold Spring Harbor, NY. 201–236.

Lake, J. A. 1985. Evolving ribosome structure: domains in archaebacteria, eubacteria, eocytes and eukaryotes. *Annu. Rev. Biochem.* 54:507–530.

Meisenberger, O., I. Pilz, M. Stöffler-Meilicke, and G. Stöffler. 1984. Small-angle x-ray study of the 50S ribosomal subunit of Escherichia coli: a comparison with different models. *Biochim. Biophys. Acta.* 781:225–233.

Oakes, M., E. Henderson, A. Scheinman, M. Clark, and J. A. Lake. 1986. Ribosome structure, function, and evolution: mapping ribosomal RNA, proteins, and functional sites in three dimensions. *In* Structure, Function and Genetics of Ribosomes. B. Hardesty and G. Kramer, editors. Springer-Verlag, New York. 47–67.

Ofengand, J., J. Ciesiolka, R. Denman, and K. Nurse. 1986. Structural and functional interactions of the tRNA-ribosome complex. *In* Structure, Function and Genetics of Ribosomes. B. Hardesty and G. Kramer, editors. Springer-Verlag, New York. 473–494.

Olson, H. M., P. G. Grant, B. S. Cooperman, and D. G. Glitz. 1982. Immunoelectron microscopic localization fo puromycin binding on the large subunit of the Escherichia coli ribosome. *J. Biol. Chem.* 257:2649–2656.

Paulsen, H., J. M. Robertson, and W. J. Wintermeyer. 1983. Topological arrangement of two transfer RNAs on the ribosome. Fluorescence energy transfer measurements between A and P-site bound tRNAphe. *J. Mol. Biol.* 167:411–426.

Radermacher, M., and J. Frank. 1984. Representation of objects reconstructed in three dimensions by surfaces of equal density. *J. Micros.* 136:77–85.

Radermacher, M., T. Wagenknecht, A. Verschoor, and J. Frank. 1987*a*. Three-dimensional structure of the large ribosomal subunit from Escherichia coli. *EMBO (Eur. Mol. Biol. Organ.) J.* 6:1107–1114.

Radermacher, M., T. Wagenknecht, A. Verschoor, and J. Frank. 1987*b*. Three-dimensional reconstruction from a single-exposure random conical tilt series applied to the 50S ribosomal subunit of Escherichia coli. *J. Microsc.* 146:113–136.

Radermacher, M., J. Frank, and T. Wagenknecht. 1988. The probable exit site of the polypeptide in the ribosome: analysis of densities in three-dimensional reconstruction. *In* Proceedings of the 9th European Congress on Electron Microscopy. H. G. Dickinson and P. J. Goodhew, editors. *Inst. Phys. Conf. Ser.* 3:323–324.

Robertson, J. M., and W. J. Wintermeyer. 1981. Effect of translocation on topology and conformation of anticodon and D loops of tRNAphe. *J. Mol. Biol.* 151:57–79.

Ryabova, L. A., O. M. Selivanova, V. I. Baranov, V. D. Vasiliev, and A. S. Spirin. 1988. Does the channel for nascent peptide exist inside the ribosome? Immune electron microscopy study. *FEBS (Fed. Eur. Biochem. Soc.) Lett.* 226:255–260.

Saxton, W. O., and W. Baumeister. 1982. The correlation averaging of a regularly arranged bacterial envelope protein. *J. Microsc.* 127:127–138.

Spirin, A. S. 1983. Location of tRNA on the ribosome. *FEBS (Fed. Eur. Biochem. Soc.) Lett.* 156:217–221.

Spirin, A. S. 1985. Ribosomal translocation: facts and models. *Prog. Nucleic Acids Res. Mol. Biol.* 32:75–114.

Stöffler, G., and M. Stöffler-Meilicke. 1983. The ultrastructure of macromolecular complexes studied with antibodies. *In* Modern Methods in Protein Chemistry. H. Tschesche, editor. de Gruyter, New York. 409–455.

Stöffler, G., and M. Stöffler-Meilicke. 1984. Immunoelectron microscopy of ribosomes. *Annu. Rev. Biophys. Bioeng.* 13:303–330.

Stöffler, G., and M. Stöffler-Meilicke. 1986. Immunoelectron microscopy on Escherichia coli ribosomes. *In* Structure, Function and Genetics of Ribosomes. B. Hardesty and G. Kramer, editors. Springer-Verlag, New York. 28–46.

Tardieu, A., and P. Vachette. 1982. Analysis of models of irregular shape by solution x-ray scattering: the case of the 50S ribosomal subunit from *E. coli*. *EMBO (Eur. Mol. Biol. Organ.) J.* 1:35–40.

van Heel, M., and J. Frank. 1981. Use of multivariate statistics in analyzing images of biological macromolecules. *Ultramicroscopy*. 6:187–194.

van Heel, M., W. Keegstra, W. Schutter, and E. F. G. van Bruggen. 1983. Arthropod hemocyanin structures studied by image analysis. *In* Structure and Function of Invertebrate Respiratory Proteins. E. G. Wood, editor. Harwood Academic Publishers, New York. 89–73.

Vasiliev, V. D. 1974. Morphology of the ribosomal 30S subparticle according to electron microscopy data. *Acta Biol. Med. Germ.* 33:779–793.

Vasiliev, V. D., O. M. Selivanova, V. I. Baranov, and A. S. Spirin. 1983.

Structural study of translating ribosomes from Escherichia coli. I. Electron microscopy. *FEBS (Fed. Eur. Biochem. Soc.) Lett.* 155:167–172.

Verschoor, A., J. Frank, T. Wagenknecht, and M. Boublik. 1986. Computer-averaged views of the 70S monosome from Escherichia coli. *J. Mol. Biol.* 187:581–590.

Wagenknecht, T., M. Radermacher, and J. Frank. 1987. Three-dimensional reconstruction of the ribosome from Escherichia coli. *In* Fifth Conversation in Biomolecular Stereodynamics. R. H. Sarma, editor. Institute of Biomolecular Stereodynamics, Albany. 251–252.

Wagenknecht, T., R. Grassucci, and J. Frank. 1988a. Electron microscopy and computer image averaging of ice-embedded large ribosomal subunits from Escherichia coli. *J. Mol. Biol.* 199:137–147.

Wagenknecht, T., J. Frank, M. Boublik, K. Nurse, and T. Ofengand. 1988b. Direct localization of the tRNA-anticodon interaction site on the Eschichia coli 30S ribosomal subunit by electron microscopy and computerized image averaging. *J. Mol. Biol.* 203:753–760.

Westerman, P., R. Benndorf, G. Lutsch, H. Bielka, and O. Nygård. 1986. Arrangement of eukaryotic initiation factor 3 and messenger RNA within preinitiation complexes. *In* Structure, Function and Genetics of Ribosomes. B. Hardesty and G. Kramer, editors. Springer-Verlag, New York. 642–657.

Wittman, H. G. 1983. Architecture of prokaryotic ribosomes. *Annu. Rev. Biochem.* 52:35–65.

Yonath, A., and H. G. Wittman. 1988. Approaching the molecular structure of ribosomes. *Biophys. Chem.* 29:17–29.

Yonath, A., K. R. Leonard, and H. G. Wittman. 1987. A tunnel in the large ribosomal subunit revealed by three-dimensional reconstruction. *Science (Wash. DC).* 236:813–816.

Zhang, N.-Y., T. Wagenknecht, M. Radermacher, T. Obrig, and J. Frank. 1987. Three-dimensional reconstruction of the 40S ribosomal subunit from rabbit reticulocytes. *In* Proceedings of the 45th Meeting of the Electron Microscopy Society of America. San Francisco Press, Inc., San Francisco. 936–937.